Check for updates

View Article Online
View Journal

PCCP

Physical Chemistry Chemical Physics

Accepted Manuscript

This article can be cited before page numbers have been issued, to do this please use: W. Yang, M. Zhao, X. Ding, K. Ma, C. Wu, I. D. Gates and Z. Gao, *Phys. Chem. Chem. Phys.*, 2020, DOI: 10.1039/C9CP05349B.

Volume 19
Number 1
7 January 2017
Pages 1-896

PCCP
Physical Chemistry Chemical Physics
rsc.li/pccp

ISSN 1463-9076

ROYAL SOCIETY OF CHEMISTRY

PAPER
H.-P. Loock *et al.*
Determination of the thermal, oxidative and photochemical degradation rates of scintillator liquid by fluorescence EEM spectroscopy

This is an Accepted Manuscript, which has been through the Royal Society of Chemistry peer review process and has been accepted for publication.

Accepted Manuscripts are published online shortly after acceptance, before technical editing, formatting and proof reading. Using this free service, authors can make their results available to the community, in citable form, before we publish the edited article. We will replace this Accepted Manuscript with the edited and formatted Advance Article as soon as it is available.

You can find more information about Accepted Manuscripts in the Information for Authors.

Please note that technical editing may introduce minor changes to the text and/or graphics, which may alter content. The journal's standard Terms & Conditions and the Ethical guidelines still apply. In no event shall the Royal Society of Chemistry be held responsible for any errors or omissions in this Accepted Manuscript or any consequences arising from the use of any information it contains.

ROYAL SOCIETY OF CHEMISTRY

rsc.li/pccp

View Article Online
DOI: 10.1039/C9CP05349B

Physical Chemistry Chemical Physics

ARTICLE

Effect of coordination environment on the kinetic and thermodynamic stability of single-atom iron catalysts

Weijie Yang[a*], Mingliang Zhao[a], Xunlei Ding[b], Kai Ma[a], Chongchong Wu[c], Ian D.Gates[c] and Zhengyang Gao[a*]

Received 00th January 20xx,
Accepted 00th January 20xx

DOI: 10.1039/x0xx00000x

www.rsc.org/

The stability of a single-atom catalyst is directly related to its preparation and application, especially for high-loading single-atom catalysts. Here, the effect of coordination environment induced by nitrogen (N) atoms coordinated with iron on the kinetic and thermodynamic stabilities of single-atom iron catalysts supported with carbon-based substrates (Fe_{SA}/CS) were investigated by density functional theory (DFT) calculations. Five Fe_{SA}/CS with different numbers of N atoms were modelled. Kinetic stability was evaluated by analyzing the migration paths of iron atom and energy barrier. The thermodynamic stability was studied by calculating the adsorption and formation energies. Our results indicated that the coordination environment induced by N can promote the kinetic and thermodynamic stability of Fe_{SA}/CS. N atoms on the substrate promote the kinetic stability by raising the energy barrier for iron migration and not only raises the thermodynamic stability, but also contributes to catalyst synthesis. Doping N on the substrate enhances charge transfer between the iron atom and substrate simultaneously improving kinetic and thermodynamic stabilities. This theoretical research provides guidance for synthesizing stable and high loading single-atom catalysts by tuning the coordination environment of the single-atom element.

1. Introduction

Single-atom catalysts (SACs) have raised extensive attention for their high catalytic activity and selectivity [1-7]. Due to its large specific surface area, excellent conductivity, and the unique physicochemical properties of carbon-based materials, SACs supported with carbon-based substrates (SACs/CS) have been widely studied in preparation, characterization, and catalytic performance by density functional theory (DFT) studies [8-12].

There are several SACs/CS experimental studies that have been reported in previous works[8, 13, 14]. Wu et al. developed a general top-down strategy for almost 30 kinds of SACs/CS, based on the pyrolysis of metal organic framework (MOF) materials [14, 15]. He et al. prepared twenty-four SACs/CS by pyrolyzing tetraphenylporphyrin and metalloporphyrin with a precursor-dilution strategy [16]. However, the preparation of high loading SACs/CS is still a challenge, especially for those SACs/CS with the loading over 5% [14]. Currently, low metal loading is an important factor that hinders the catalytic performance [17, 18]. Therefore, developing high loading SACs/CS is a main challenge for experimental preparations.

To achieve high loading of SACs, substrates must firmly anchor the metal atoms, in order to avoid migration and agglomeration. In the system of metal oxide substrates, the vacancy of cation or oxygen can hold metal atoms firmly through a strong covalent metal–support interaction [19-21]. However, in the system of carbon-based substrates, the investigation on the interaction between metal atom and carbon-based substrates is insufficient. Based on the previous research on metal oxides substrates, the coordination environment of the metal atom is directly related to the stability of the SACs [22]. In the system of carbon-based substrates, the coordination environment of the metal atom includes the coordination number and coordinated atoms. Zhou et al. studied the effect of coordination number on the stability and catalytic activity of the water splitting reaction by using DFT calculations [23]. Gao et al. investigated the effect of coordination number on catalytic activity and selectivity in hydrogen and oxygen evolution reactions [24]. However, there was a lack of systematic investigation on the effect of coordination environment dominated by coordinated atoms on the stability of SACs/CS. In an experimental study of catalyst preparation, Wu et al. prepared three kinds of four-coordinated single-atom cobalt catalysts with different N atom numbers by regulating calcination temperature and found that the three kinds of cobalt catalysts with different numbers of N atoms exhibited significant differences of the catalytic activity in CO_2 electroreduction [25]. Therefore, it is particularly important to study the effects of coordination environment dominated by the doped atom on the stability of SACs/CS.

To discuss the effect of coordination environment on the single-atom dopant, we chose single-atom iron catalysts supported with carbon-based substrates (Fe_{SA}/CS) as an example, due to its excellent performance in many catalytic reactions including methane

---

[a] School of Energy and Power Engineering, North China Electric Power University, Baoding 071003, China.
[b] School of Mathematics and Physics, North China Electric Power University, Beijing 102206, China.
[c] Department of Chemical and Petroleum Engineering, University of Calgary, T2N 1N4, Calgary, Alberta, Canada.
E-mail: yangwj@ncepu.edu.cn and gaozhyan@163.com.

conversion [26, 27], oxygen reduction [17], and nitrogen reduction [11]. Considering that Fe_{SA}/CS with double-vacancy carbon-based substrates have been successfully prepared by experimental research [28-32], a double vacancy carbon-based substrate was selected in this study. In addition, the doping of N into carbon-based substrate is one of the most common methods for modification of Fe_{SA}/CS, thus we modeled five Fe_{SA}/CS with varying numbers of N atoms, to analyze the effect of coordination environment on the stability of Fe_{SA}/CS. The stability of SACs/CS embodies two aspects: i) thermal stability and ii) kinetic stability. In theory, thermal stability can be measured through the adsorption energy of metal atom [33] and deformation energy of SACs/CS [34] whereas kinetic stability can be analyzed by examining the energy barrier of the transfer process of the metal atom [35].

2. Calculation method

All the DFT calculations were performed with Vienna *ab initio* simulation (VASP 5.4.1) package [36, 37]. The Perdew, Burke, and Ernzernhof (PBE) functional with projector augmented wave (PAW) basis set was used to describe the interactions between core and valence electrons [38]. To obtain more accurate interactions between iron atom and substrates, spin polarization and Van Der Waals interactions were included in the analysis. DFT-D3 correction was applied to study weak intermolecular interactions [39]. Consistent with previous researchers [33, 40-42], the cutoff of the kinetic energy for the projector augmented wave basis set and Gaussian smearing were selected at 500 eV and 0.05 eV, respectively. Based on a 4×4 supercell graphene, the theoretical calculation model with a 15 Å vacuum layer was constructed [43, 44]. For geometry optimization, the energy and force convergence standards were set equal to 10^{-5} eV[45] and 0.02 eV/Å[46], respectively. For reaction path search and potential energy surface location, the CI-NEB method with eight image points was applied [47, 48]. A 7×7×1 Γ-centered k-point grid was used in geometry optimization, and a 15×15×1 Γ-centered k-point grid was used to ensure a self-consistent field to obtain accurate electronic energy in ground state.

To evaluate the difficulty in the formation of Fe_{SA}/CS, the formation energy was calculated, according to the following equation:

$$E_f = E_{Fe/CS} + x\mu_C - y\mu_N - E_G - E_{Fe} \quad (1)$$

where $E_{Fe/CS}$ is the total energy of M/GS, x is the number of carbon atoms removed from the pristine graphene; μ_C is the chemical potential of carbon defined as the total energy per carbon atom for pristine graphene, y is the number of nitrogen atoms added, μ_N is the chemical potential of nitrogen (defined as half of the total energy of a N_2 molecule), E_G is the total energy of perfect graphene, and E_{Fe} is the total energy of an isolated iron atom in the vacuum.

To investigate the interaction between iron atom and substrates, the adsorption energy (E_a) was calculated according to the following equation:

$$E_a = E_{Fe/CS} - E_{Sub} - E_{Fe} \quad (2)$$

where E_{Sub} is the total energy of double vacancy carbon-based substrate.

To measure the difficulty of iron atom migration, the energy barrier (E_b) was calculated, according to the following equation:

$$E_b = E_{TS} - E_{IS} \quad (3)$$

where E_{TS} is the total energy of transition state configuration and E_{IS} is the total energy of initial configuration.

View Article Online
DOI: 10.1039/C9CP05349B

3. Results and discussion

3.1 Catalyst model

Five Fe_{SA}/CS with different N atoms, from zero to five, were constructed with different coordination environments all with the same coordination number. The geometric structures of double vacancy carbon-based substrate and five Fe_{SA}/CS with different N atoms were plotted, as shown in Fig. 1. From Fig. 1(b) to (f), the number of N atoms in Fe_{SA}/CS increased from zero to four. The key bond lengths were summarized in Table1, which are consistent with previous studies.

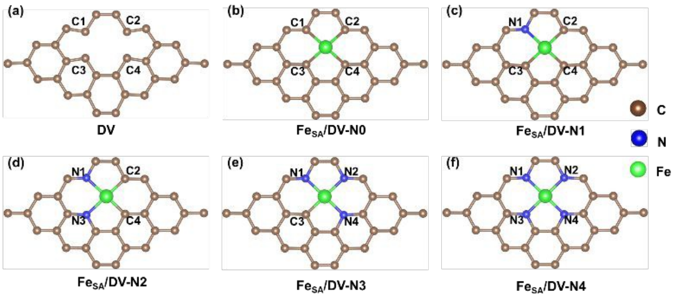

Fig. 1 Fe_{SA}/CS and N atoms configuration cases

Table 1 Bond lengths of double vacancy substrate and five single-atom iron catalysts

Structures	Bond lengths (Å)			
DV	C1-C2	C2-C3	C3-C4	C4-C1
	3.03	1.91	3.03	1.91
Fe_{SA}/DV-N0	Fe-C1	Fe-C2	Fe-C3	Fe-C4
	1.96 (1.96 [49])	1.96 (1.96 [49])	1.96 (1.96 [49])	1.96 (1.96 [49])
Fe_{SA}/DV-N1	Fe-N1	Fe-C2	Fe-C3	Fe-C4
	1.99	1.93	1.91	1.94
Fe_{SA}/DV-N2	Fe-N1	Fe-C2	Fe-N3	Fe-C4
	1.96	1.86	1.96	1.86
Fe_{SA}/DV-N3	Fe-N1	Fe-N2	Fe-C3	Fe-N4
	1.88	1.93	1.92	1.87
Fe_{SA}/DV-N4	Fe-N1	Fe-N2	Fe-N3	Fe-N4
	1.89 (1.89[41])	1.89 (1.89[41])	1.89 (1.89[41])	1.89 (1.89[41])

In addition, spin density and magnetic moment of five Fe_{SA}/CS were calculated (Fig. S1), and the unpaired electron distribution mainly distributed around the iron atom, indicating that Fe atom is active site. Moreover, decomposed charge density near Fermi energy level of five Fe_{SA}/CS were calculated, as shown in Fig. S2. Similar to the spin density, the charge density near Fermi energy level mainly located at Fe atom, confirming that Fe atom is the catalytic centre and the calculated results are reasonable.

3.2 Analysis of kinetic stability

3.2.1 Possible migration paths

To determine migration paths of iron metal on the five different Fe_{SA}/CS cases, we designed five possible migration paths, as shown in Fig. 2. In Fig.2, the five possible transfer sites of iron atom are labeled in red number. The final geometric structures and relative energies of the five different migration paths are plotted in Figs. S3 to S7. There were three possible transfer sites in Fe_{SA}/DV-N0 and Fe_{SA}/DV-N4 due to their system symmetry. By comparing the relative energies between initial and final geometric structures, the most thermodynamically stable final geometric structures were found. In addition, the most possible migration paths for the five Fe_{SA}/CS cases were identified and labeled with red arrows. From the results, the relative energies for the five Fe_{SA}/CS cases were 4.59, 5.53, 5.51, 5.89, and 5.94 eV, respectively. When iron atoms transfer from vacancy defects to the graphene surface, they are likely to agglomerate with each other to form clusters or nanoparticles.

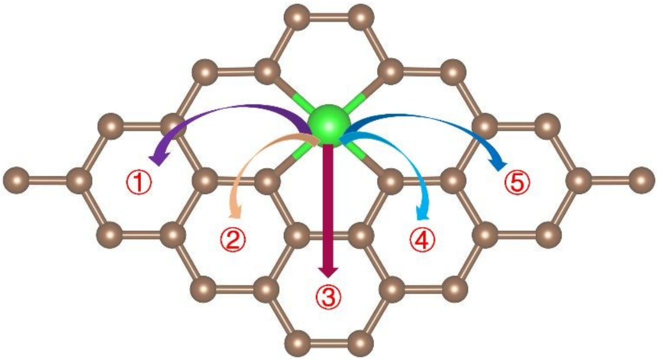

Fig. 2 Five possible migration paths and transfer sites of Fe atom

3.2.2 Analysis of reaction paths

Based on the above discussions on the migration paths, the reaction paths and transition state structures of iron atom migration for the five Fe_{SA}/CS cases were calculated, as shown in Figs. 3-7. Considering that there were significant energy variation and height variation of the iron atom in the migration reaction, the energy variation, height variation of iron atom, and key configuration (side and top views) are examined. To analyze the energy and height variations of the iron atom, the initial configuration energy and iron atom height were taken as the energy and height reference states. For example, the Fe_{SA}/DV-N0, as shown in Fig. 3, the height of iron atom enlarges as the migration reaction proceeds. Simultaneously, the energy increases with the rise of iron atom height. However, it should be noted that the maximum of the energy and iron atom height are not in the same configuration. For the other four Fe_{SA}/CS cases, the migration reaction of the iron atom is similar to that in Fe_{SA}-DV-N0. The energy barriers of iron atom migration in the five Fe_{SA}/CS cases are 5.03, 5.73, 5.87, 6.05, and 6.31 eV, respectively, which are similar to that of Mn (4.87 eV [35] and 5.91 eV [50]) and Pd (4.08 eV [51]), suggesting that the calculated results are reasonable. The calculated transfer energy barriers of Fe atom are obviously larger than the general chemical reaction, which is an exactly desirable property in the system of SACs to guarantee the stability of catalysts. In addition, the maximum relative heights of iron atom of the five Fe_{SA}/CS cases are 1.33, 1.62, 1.91, 2.10, and 2.39 Å, respectively. Moreover, the coordinates of initial, transition state and final configurations were provided in Table S1 to S5.

View Article Online
DOI: 10.1039/C9CP05349B

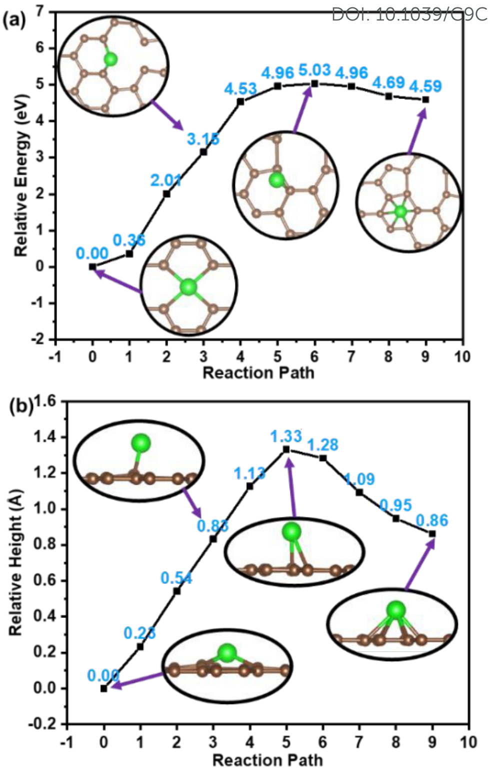

Fig. 3 (a) Energy variation and key configurations (in top view) along the reaction path in Fe_{SA}/DV-N0 and (b) Height variation and key configurations (in side view) along the reaction path in Fe_{SA}/DV-N0

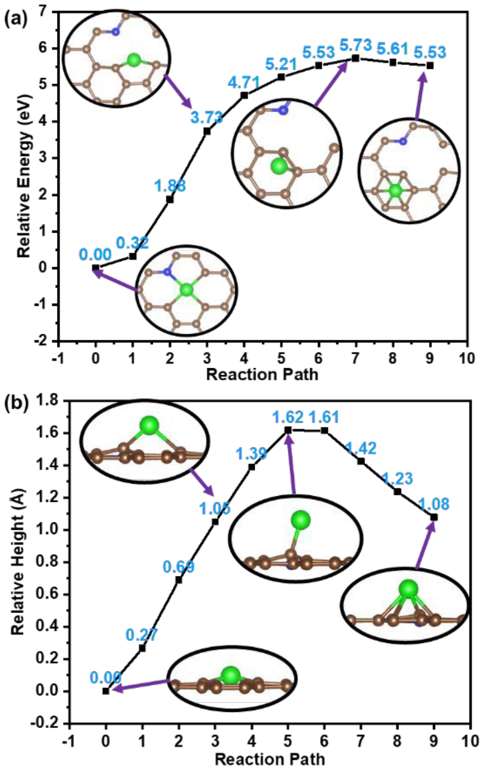

Fig. 4 (a) Energy variation and key configurations (in top view) along the reaction path in Fe_{SA}/DV-N1 and (b) Height variation

View Article Online
DOI: 10.1039/C9CP05349B

and key configurations (in side view) along the reaction path in Fe_{SA}/DV-N1

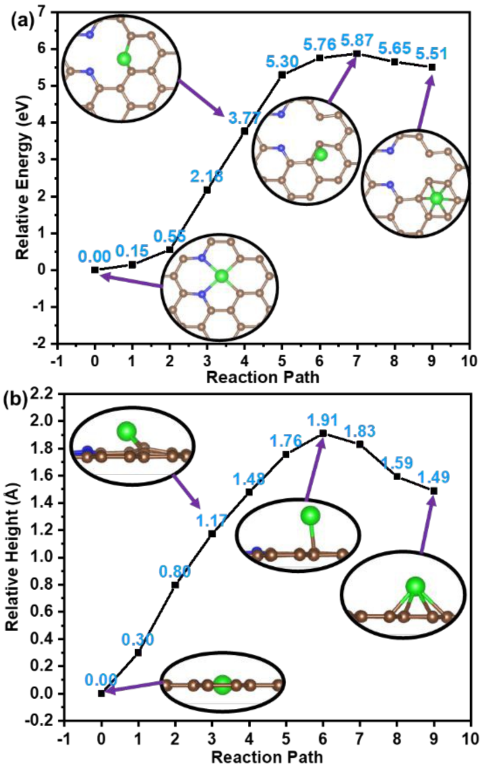

Fig. 5 (a) Energy variation and key configurations (in top view) along the reaction path in Fe_{SA}/DV-N2 and (b) Height variation and key configurations (in side view) along the reaction path in Fe_{SA}/DV-N2

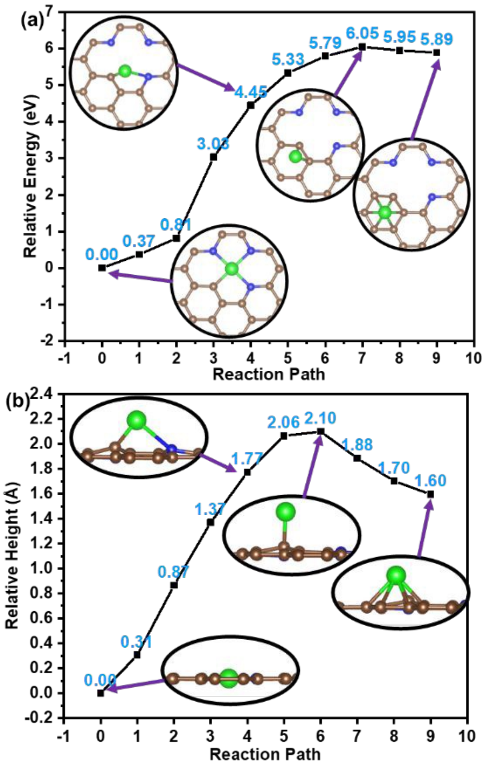

Fig. 6 (a) Energy variation and key configurations (in top view) along the reaction path in Fe_{SA}/DV-N3 and (b) Height variation and key configurations (in side view) along the reaction path in Fe_{SA}/DV-N3

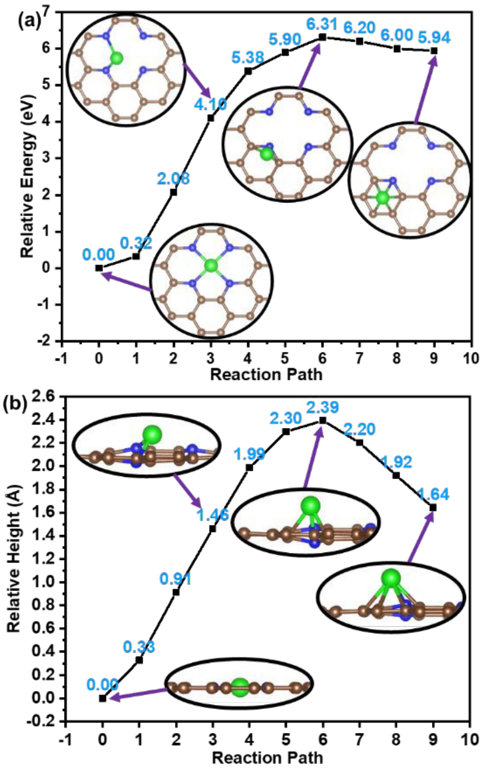

Fig. 7 (a) Energy variation and key configurations (in top view) along the reaction path in Fe_{SA}/DV-N4 and (b) Height variation and key configurations (in side view) along the reaction path in Fe_{SA}/DV-N4

To further investigate the effect of doping N atoms on the kinetic stability, the energy barrier of the migration process of the iron atom was calculated according to Equation (3). The relationship between energy barrier and number of N atom and the relationship between maximum relative height of iron atom and number of N atom were calculated, as shown in Fig. 8. The results show that there is a linear relationship between the energy barrier of iron atom migration and number of N atoms, with a correlation coefficient (R^2) equal to 0.90, suggesting that doping N atoms into substrates can promote the kinetic stability of Fe_{SA}/CS by raising the energy barrier of iron atom migration. Furthermore, a linear relationship was also evident between the maximum relative height in the iron atom migration process and number of N atoms, with a R^2 of 0.91, suggesting that doping N atoms into substrates raises the energy barrier of iron atom migration by increasing the elevation of iron atom in migration reaction. The higher the elevation of iron atom, the stronger is the interaction between the iron atom and substrate which has to be overcome, and thus, the larger is the reaction barrier. Therefore, according to our results, the coordination environment has a significant effect on kinetic stability, and furthermore, we can regulate the kinetic stability by tuning the number of N atoms coordinated with iron. In addition, In addition, to verify that the calculation results are independent of the model size, take the system of Fe_{SA}/DV-N4 as an example, we calculated the charge and transfer energy barrier of Fe atom in the supercell of 4×4, 5×5 and 6×6, as shown in Fig. S8. Obviously, there was no significant variation in the calculated charge and transfer energy barrier of Fe atom with 4×4, 5×5 and 6×6 supercell, suggesting that our calculated results should be independent of the model size, and the conclusion should be general.

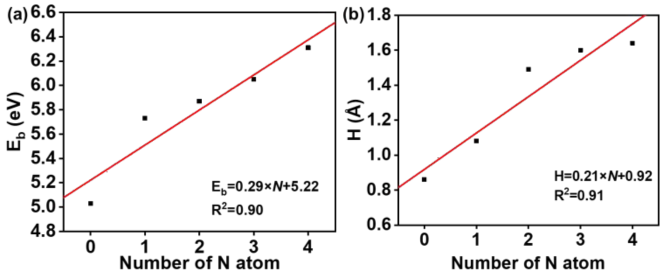

Fig. 8 Energy barrier and maximum relative height of iron atom, with the function of the number of N

3.3 Analysis of thermodynamic stability

To analyze the effect of coordination environment on thermodynamic stability, the adsorption energy of iron atom (E_a) and formation energy of Fe_{SA}/CS (E_f) were calculated according to Equations (1) and (2) (Fig. 9). In Fig. 9(a), the adsorption energy of iron atom in Fe_{SA}/DV-N0 is -6.12 eV, which is significantly less than another four Fe_{SA}/CS with N atom doped, suggesting that doping N atoms into substrates promote the interaction between iron atom and substrates. In Fig. 9(b), the formation energy of Fe_{SA}/DV-N0 is 2.06 eV, suggesting that the formation of Fe_{SA}/DV-N0 requires large external energy input. According to the research of Robertson et al. [52], Fe_{SA}/DV-N0 can be prepared through focused electron beam irradiation at 80 kV, which is consistent with a positive formation energy. In addition, the formation energy of Fe_{SA}/DV-N4 is -3.26 eV, suggesting that the formation energy does not require external energy. According to the research of Deng et al. [12], Fe_{SA}/DV-N4 can be prepared through high-energy ball milling (a mechanical process), which is consistent with a negative formation energy. Furthermore, the formation energies of the five Fe_{SA}/CS cases drop gradually with the increase of the number of doped N atoms, suggesting that nitrogen-coordinated Fe_{SA}/CS is facile be synthesized. Therefore, the coordination environment has a significant effect on thermodynamic stability of Fe_{SA}/CS, and we can regulate the interaction between iron atom and substrate and the synthesis difficulty through tuning the number of N atoms coordinated with the iron atom.

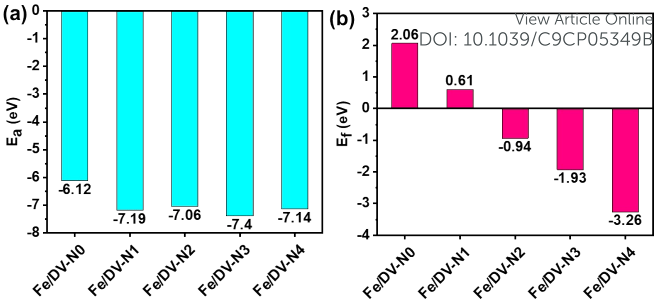

View Article Online
DOI: 10.1039/C9CP05349B

Fig. 9 (a) Adsorption energies of Fe atom on five Fe_{SA}/CS. (b) Formation energies of five Fe_{SA}/CS

3.4 Analysis of binding mechanism

According to the above discussions on the kinetic and thermodynamic stabilities, we conclude that the number of N atoms coordinated by iron atom is directly related to the kinetic and thermodynamic stability of Fe_{SA}/CS. To further explore the essential relevance between the coordination environment and stability, the binding mechanisms of iron atom on substrates in five Fe_{SA}/CS were investigated. According to previous studies [41, 53, 54], there were two main contributions to the binding interaction in the gas adsorption system of Fe_{SA}/CS, including covalent bond contributions dominated by orbital hybridization and ionic bond contributions dominated by charge transfer[55]. Therefore, we calculated the projected density of states (PDOS) of the five Fe_{SA}/CS cases and charge variation of the iron atom to analyze orbital hybridization effects and charge transfer, respectively, as shown in Fig. 10.

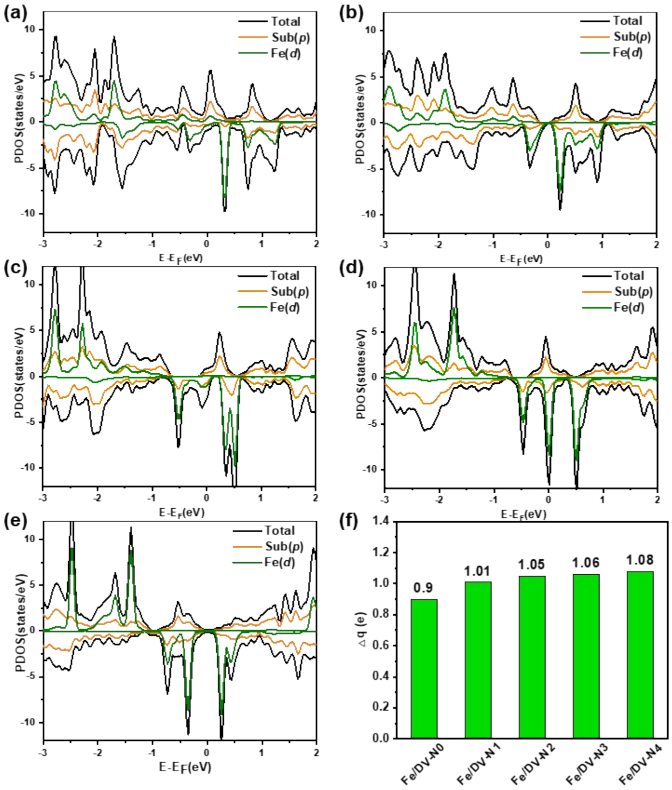

Fig. 10 (a) ~ (e) PDOS of five Fe_{SA}/CS (f) Charge transfer evaluations of five Fe_{SA}/CS

In Fig. 10(a)-(e), the total density of states, *p* orbital of the substrate, and *d* orbital of the iron atom are plotted in black, orange, and green, respectively. The results suggest no significant orbital hybridization between the *p* orbital of substrates and *d* orbital of the iron atom, suggesting that covalent bonds are not dominant in the binding process of iron atom and substrates. In Fig. 10(f), the charge variations of iron in the five Fe_{SA}/CS cases were all larger than zero, indicating that the iron atom gained electrons in the binding process. Moreover, the number of electrons obtained by the iron atom in the five Fe_{SA}/CS cases were 0.90, 1.01, 1.05, 1.06, and 1.08 e, respectively, suggesting that doping N atoms into substrates promotes the contribution of ionic bonds by facilitating charge transfer between the iron atom and substrate. Therefore, the contribution of the ionic bond dominated by charge transfer acts is more dominantly in the binding process, and doping N atoms into substrates can simultaneously improve kinetic and thermodynamic stability by enhancing charge transfer between iron atom and substrates.

Conclusions

The effect of coordination environment induced by N coordinated with an iron on the kinetic and thermodynamic stability of Fe_{SA}/CS was investigated by DFT calculations. Five Fe_{SA}/CS with different types of N, from zero to five, with different coordination environments with the same coordination number were studied. Our results indicate that doping N atoms into substrates promote kinetic stability of Fe_{SA}/CS by raising the energy barrier of iron atom migration. There was a significant linear relationship between the energy barrier and maximum relative height of iron atom in the migration process. Doping N atoms into substrates not only promotes thermodynamic stability of Fe_{SA}/CS, but also contributes to the ease of synthesis of Fe_{SA}/CS. The contributions of ionic bonds dominated by charge transfer is dominant in the binding process. According to the anchoring mechanism, the coordination environment induced by N atoms number coordinated with iron atom regulate both kinetic and thermodynamic stability by tuning the charge transfer between the iron atom and substrates, which provides guidance for synthesizing highly stable and high loading single-atom catalysts.

Conflicts of interest

There are no conflicts to declare.

Acknowledgements

This work was supported by the National Natural Science Foundation of China (No. 91545122), Beijing Natural Science Foundation (2182066) and Natural Science Foundation of Hebei Province of China (B2018502067). IDG and CCW acknowledge support from the University of Calgary's Canada First Research Excellence Fund (CFREF) program entitled the Global Research Initiative for Sustainable Low Carbon Unconventional Resources.

Notes and references

1. Y. Shi, C. Zhao, H. Wei, J. Guo, S. Liang, A. Wang, T. Zhang, J. Liu and T. Ma, *Adv. Mater.*, 2014, 26, 8147-8153.
2. X. Cui, W. Li, P. Ryabchuk, K. Junge and M. Beller, *Nat. Catal.*, 2018, **1**, 385-397.
3. X. F. Yang, A. Q. Wang, B. T. Qiao, J. Li, J. Y. Liu and T. Zhang, *Acc. Chem. Res.*, 2013, **46**, 1740-1748.
4. Y. Cheng, S. Yang, S. P. Jiang and S. Wang, *Small Methods*, 2019, 1800440.
5. H. Li, W. Chai and G. Henkelman, *J. Mater. Chem. A*, 2019, DOI: 10.1039/C9TA04572D.
6. H. Li and G. Henkelman, *J. Phys. Chem. C*, 2017, **121**, 27504-27510.
7. H. Li, K. Shin and G. Henkelman, *J. Chem. Phys.*, 2018, **149**, 174705.
8. Y. Peng, B. Lu and S. Chen, *Adv. Mater.*, **0**, 1801995.
9. C. Rivera-Cárcamo and P. Serp, *ChemCatChem*, 2018, **10**, 5058-5091.
10. W. Liu, Y. Chen, H. Qi, L. Zhang, W. Yan, X. Liu, X. Yang, S. Miao, W. Wang, C. Liu, A. Wang, J. Li and T. Zhang, *Angew. Chem., Int. Ed.*, 2018, **57**, 7071-7075.
11. Y. Wang, X. Cui, J. Zhao, G. Jia, L. Gu, Q. Zhang, L. Meng, Z. Shi, L. Zheng, C. Wang, Z. Zhang and W. Zheng, *ACS Catal.*, 2018, 336-344.
12. D. Deng, X. Chen, L. Yu, X. Wu, Q. Liu, Y. Liu, H. Yang, H. Tian, Y. Hu and P. Du, *Sci. Adv.*, 2015, **1**, e1500462.
13. A. Han, B. Wang, A. Kumar, Y. Qin, J. Jin, X. Wang, C. Yang, B. Dong, Y. Jia, J. Liu and X. Sun, *Small Methods*, 2019, 1800471.
14. Z. Li, D. Wang, Y. Wu and Y. Li, *Natl. Sci. Rev.*, 2018, **5**, 673-689.
15. J. Wang, Z. Li, Y. Wu and Y. Li, *Adv. Mater.*, 2018, **30**, 1801649.
16. X. He, Q. He, Y. Deng, M. Peng, H. Chen, Y. Zhang, S. Yao, M. Zhang, D. Xiao, D. Ma, B. Ge and H. Ji, *Nat. Commun.*, 2019, **10**, 3663.
17. L. Jiao, G. Wan, R. Zhang, H. Zhou, S.-H. Yu and H.-L. Jiang, *Angew. Chem., Int. Ed.*, 2018, **57**, 8525-8529.
18. P. Liu, Y. Zhao, R. Qin, S. Mo, G. Chen, L. Gu, D. M. Chevrier, P. Zhang, Q. Guo, D. Zang, B. Wu, G. Fu and N. Zheng, *Science*, 2016, **352**, 797-800.
19. J.-C. Liu, Y. Tang, Y.-G. Wang, T. Zhang and J. Li, *Natl. Sci. Rev.*, 2018, **5**, 638-641.
20. B. Qiao, J.-X. Liang, A. Wang, C.-Q. Xu, J. Li, T. Zhang and J. J. Liu, *Nano Research*, 2015, **8**, 2913-2924.
21. H. Li, L. Luo, P. Kunal, C. S. Bonifacio, Z. Duan, J. C. Yang, S. M. Humphrey, R. M. Crooks and G. Henkelman, *J. Phys. Chem. C*, 2018, **122**, 2712-2716.
22. Y.-Q. Su, Y. Wang, J.-X. Liu, I. A. W. Filot, K. Alexopoulos, L. Zhang, V. Muravev, B. Zijlstra, D. G. Vlachos and E. J. M. Hensen, *ACS Catal.*, 2019, **9**, 3289-3297.
23. Y. Zhou, G. Gao, Y. Li, W. Chu and L. W. Wang, Phys. Chem. Chem. Phys., 2019, 21, 3024-3032.
24. G. Gao, S. Bottle and A. Du, Catal. Sci. Technol., 2018, 8, 996-1001.
25. W. Xiaoqian, C. Zhao, Z. Xuyan, Y. Tao, C. Wenxing, Y. Rui, Z. Changming, W. Geng, W. Jing, H. Weixin, Y. Jinlong, H. Xun, W. Shiqiang, W. Yuen and L. Yadong, Angew. Chem., Int. Ed., 2018, 130, 1962-1966.
26. X. Cui, H. Li, Y. Wang, Y. Hu, L. Hua, H. Li, X. Han, Q. Liu, F. Yang, L. He, X. Chen, Q. Li, J. Xiao, D. Deng and X. Bao, Chem, 2018, 4, 1–9.
27. C. Wu and I. D. Gates, Molecular Catalysis, 2019, 469, 40-47.

28. Y. Pan, Y. Chen, K. Wu, Z. Chen, S. Liu, X. Cao, W. C. Cheong, T. Meng, J. Luo, L. Zheng, C. Liu, D. Wang, Q. Peng, J. Li and C. Chen, *Nat. Commun.*, 2019, **10**, 4290.

29. W. L. Wang, E. J. Santos, B. Jiang, E. D. Cubuk, C. Ophus, A. Centeno, A. Pesquera, A. Zurutuza, J. Ciston, R. Westervelt and E. Kaxiras, *Nano Lett.*, 2014, **14**, 450-455.

30. W. Liu, L. Zhang, X. Liu, X. Liu, X. Yang, S. Miao, W. Wang, A. Wang and T. Zhang, *J. Am. Chem. Soc.*, 2017, **139**, 10790−10798.

31. H. Fei, J. Dong, Y. Feng, C. S. Allen, C. Wan, B. Volosskiy, M. Li, Z. Zhao, Y. Wang, H. Sun, P. An, W. Chen, Z. Guo, C. Lee, D. Chen, I. Shakir, M. Liu, T. Hu, Y. Li, A. I. Kirkland, X. Duan and Y. Huang, *Nat. Catal.*, 2018, **1**, 63-72.

32. C. Zhang, S. Yang, J. Wu, M. Liu, S. Yazdi, M. Ren, J. Sha, J. Zhong, K. Nie, A. S. Jalilov, Z. Li, H. Li, B. I. Yakobson, Q. Wu, E. Ringe, H. Xu, P. M. Ajayan and J. M. Tour, *Adv. Energy Mater.* 2018, 1703487.

33. Z. Y. Gao, W. J. Yang, X. L. Ding, G. Lv and W. P. Yan, *Phys. Chem. Chem. Phys.*, 2018, **20**, 7333-7341.

34. J. Zhang, Y. Wang, Y. Wang and M. Zhang, *J. Electrochem. Soc.*, 2017, **164**, F1122-F1129.

35. L. Xu, L.-M. Yang and E. Ganz, *Theor. Chem. Acc.*, 2018, **137**.

36. G. Kresse and J. Furthmüller, *Comput. Mater. Sci.*, 1996, **6**, 15-50.

37. G. Kresse and J. Furthmüller, *Phys. Rev. B*, 1996, **54**, 11169.

38. J. P. Perdew, K. Burke and M. Ernzerhof, *Phys. Rev. Lett.*, 1996, **77**, 3865.

39. S. Grimme, J. Antony, S. Ehrlich and H. Krieg, *J. Chem. Phys.*, 2010, **132**, 154104.

40.W. Yang, S. Xu, M. Kai, C. Wu, I. D. Gates, X. Ding, W. Meng and Z. Gao, *Nano Materials Science*, 2019, DOI: https://doi.org/10.1016/j.nanoms.2019.10.008.

41. W. Yang, Z. Gao, X. Liu, X. Li, X. Ding and W. Yan, *Catal. Sci. Technol.*, 2018, **8**, 10.

42. W. Yang, Z. Gao, X. Ding, G. Lv and W. Yan, *Appl. Surf. Sci.*, 2018, **455**, 940-951.

43. L. B. Shi, Y. P. Wang and H. K. Dong, *Appl. Surf. Sci.*, 2015, **329**, 330-336.

44. M. D. Esrafili and S. Heydari, *ChemistrySelect*, 2018, **3**, 4471-4479.

45. Y. Tang, W. Chen, C. Li, L. Pan, X. Dai and D. Ma, *Appl. Surf. Sci.*, 2015, **342**, 191-199.

46. Y. Tang, W. Chen, Z. Shen, C. Li, D. Ma and X. Dai, *Phys. Chem. Chem. Phys.*, 2018, **20**, 2284-2295.

47. G. Henkelman, B. P. Uberuaga and H. Jónsson, *J. Chem. Phys.*, 2000, **113**, 9901-9904.

48. G. Henkelman and H. Jónsson, *J. Chem. Phys.*, 2000, **113**, 9978-9985.

49. A. V. Krasheninnikov, P. O. Lehtinen, A. S. Foster, P. Pyykko and R. M. Nieminen, *Phys. Rev. Lett.*, 2009, **102**, 126807.

50. Q. Jiang, J. Zhang, Z. Ao, H. Huang, H. He and Y. Wu, *Front. Chem.*, 2018, **6**, 187.

51. G. Xu, R. Wang, F. Yang, D. Ma, Z. Yang and Z. Lu, *Carbon*, 2017, **118**, 35-42.

52. A. W. Robertson, B. Montanari, K. He, J. Kim, C. S. Allen, Y. A. Wu, J. Olivier, J. Neethling, N. Harrison, A. I. Kirkland and J. H. Warner, *Nano letters*, 2013, **13**, 1468-1475.

53. W. Yang, Z. Gao, X. Liu, X. Ding and W. Yan, *Chem. Eng. J.*, 2019, **361**, 304-313.

54. W. Yang, Z. Gao, X. Liu, C. Ma, X. Ding and W. Yan, *Fuel*, 2019, **243**, 262-270.

55. H. Li, S. Guo, K. Shin, M. S. Wong and G. Henkelman, *ACS Catal.*, 2019, **9**, 7957−7966